Nanoscale Advances

PAPER

View Article Online
View Journal | View Issue

Cite this: *Nanoscale Adv.*, 2019, **1**, 834

Ligand-assisted reduction and reprecipitation synthesis of highly luminescent metal nanoclusters†

Yue Wang,[ab] Yu-e Shi,*[ab] Tianzi Li,[a] Henggang Wang,[a] Yanxiu Li,[c] Yuan Xiong,[c] Shan Peng [a] and Zhenguang Wang *[ab]

Solid-state luminescent materials play a key role in fabricating light-emitting diodes (LEDs). Herein, highly luminescent metal nanoclusters (NCs) are synthesized using a ligand-assisted reduction and reprecipitation process. Glutathione (GSH) dissolved in a good solvent (water) is injected into a poor solvent (ethanol in which Cu^{2+} is dissolved), where the fast reduction of Cu^{2+} by GSH and the supersaturation-induced aggregation triggered by the solubility change of GSH upon solvent mixing occur. Nanoparticles with diameters of around 50–80 nm embedded with small-sized Cu NCs (around 2 nm) can be obtained and processed into powders simply by drying the solvent. The powders show bright-orange emission with a photoluminescence quantum yield as high as 48%. Nearly monoexponential behavior was observed in the photoluminescence decay profiles of the Cu NCs, which can be attributed to the abundance of metal defect-related states formed with the assistance of coordination between Cu and ethanol. Moreover, white LEDs were fabricated using blue-emissive commercial phosphors and orange-emissive Cu NCs as color converters integrated with UV LED chips.

Received 3rd October 2018
Accepted 14th November 2018

DOI: 10.1039/c8na00268a

rsc.li/nanoscale-advances

Introduction

Solid-state luminescent materials (SLMs) have attracted significant interest for numerous applications in sensing,[1,2] bioimaging,[3,4] security printing[5,6] and light-emitting diodes (LEDs).[7–9] For LEDs, SLMs play an especially key role in determining the performance of commercial devices, such as emitting color, color temperature, and color rendering index (CRI), by acting as color-conversion layers. Most commercialized SLMs for LEDs are rare-earth element-doped materials, which exhibit high photoluminescence (PL) quantum yield (QY).[10] However, these SLMs are facing a supply shortage due to growing demand combined with their nonrenewable property.[11] Other luminescent materials such as semiconductor quantum dots (QDs) are potential alternatives; however, they often rely on heavy metals (Cd and Pb) to achieve good PL performance, leading to toxicity concerns.[9,12–14] Consequently, the development of alternative SLMs that can be easily synthesized on a large scale from non-toxic precursors as substitutes for heavy metal- and rare earth-based materials is an important research topic.

Metal nanoclusters (NCs), nano-sized metal atom cores surrounded by ligands, have emerged as promising materials due to their remarkable chemical and optical properties, including earth abundance, non-toxicity, HOMO–LUMO transition and reasonably high PL.[15–19] However, highly luminescent metal NC-based SLMs are difficult to realize because solid-state metal NCs are prone to becoming highly concentrated or even aggregated. This leads to the deterioration of their PL properties as a result of reabsorption and nonradiative energy transfer, which is known as aggregation-caused quenching. The concept of aggregation-induced emission (AIE), coined by Tang's group, provides new perspectives for designing highly luminescent SLMs that avoid aggregation-caused quenching.[20,21] We and other groups have reported SLMs using the AIE properties of Cu and Au NCs.[22–26] The enhanced emission can be ascribed to two mechanisms resulting from the promoted compactness of metal NCs: (a) enhancing the inter- and intra-NC metallophilic interactions by dealing with the metal defects on the metal NC surfaces; and (b) reducing the nonradiative relaxation of excited states by restricting the vibrations and rotations of ligands.[20,26] To achieve high compactness, an excess of poor solvent is usually mixed with the NCs in a small amount of good solvent to precipitate the luminescent materials. The aforementioned solvents are then discarded. On one hand, this operation is complicated and leads to extremely diluted NCs, making it difficult to obtain SLMs on a large scale.

[a]College of Chemistry and Environmental Science, Hebei University, Baoding, 071002, P. R. China. E-mail: wzg583@163.com

[b]Key Laboratory of Medicinal Chemistry and Molecular Diagnosis (Hebei University), Ministry of Education, Baoding, 071002, P. R. China

[c]Department of Materials Science and Engineering & Centre for Functional Photonics (CFP), City University of Hong Kong, 83 Tat Chee Avenue, Kowloon, Hong Kong SAR, China

† Electronic supplementary information (ESI) available. See DOI: 10.1039/c8na00268a

On the other hand, aggregation is driven by the difference in the ligand's solubility in good and poor solvents, which can effectively restrict the vibrations and rotations of ligands. However, the metal defects cannot be well controlled or even passivated by the excess of poor solvent.

Herein, a straightforward method (Fig. 1a) for the gram-scale synthesis of luminescent Cu NCs is developed by using a ligand-assisted reduction and reprecipitation (LARR) process to control the compactness of the Cu NCs. This process both enhances the metallophilic interactions and restricts the vibrations and rotations of ligands. The Cu NCs can then be used to produce SLMs. Glutathione (GSH) is selected as the ligand to reduce Cu^{2+} and trigger the aggregation of Cu clusters based on its difference in solubility in good and poor solvents, as confirmed by comparative studies of different ligands along with optical and structural characterizations. The PL mechanisms are studied by recording the PL decay curves of the Cu NCs at different emission wavelengths. We further demonstrated the application of the Cu NCs in the fabrication of LEDs by using the Cu NCs as light-conversion layers.

Results and discussion

Synthesis of Cu NCs *via* the LARR process

The LARR synthesis is accomplished simply by injecting good solvent (water) containing GSH into poor solvent (ethanol into which Cu^{2+} is dissolved) under vigorous stirring, as shown in Fig. 1a. Typically, 0.5 mL of saturated aqueous GSH solution is quickly injected into 9.5 mL of ethanol solution containing 5 mM Cu^{2+} under vigorous stirring. A dark black color is observed immediately upon injection and gradually turns into a milky white color, signaling the formation of Cu NCs. GSH (structure shown in Fig. 1b) acts as both a reduction reagent to lower the valence of Cu^{2+} and a trigger for aggregation based on its huge difference in solubility between water and ethanol. The solution is centrifuged at 500 krpm to remove the large yellow particles, and the supernatant solution is collected. The supernatant shows strong orange emission under UV irradiation, as shown in Fig. 1c. To understand the role of GSH in the synthetic process, contrast experiments are carried out. Ligands with structures similar to GSH, including cysteine and cysteamine, were used to synthesize Cu NCs. Upon injecting cysteamine into ethanol containing Cu^{2+}, the deep-blue solution immediately turns colorless. Upon cysteine injection, the solution becomes black. The solutions become cloudy after stirring for 5 min, indicating the reduction of Cu^{2+} by the above two ligands. However, no emission under UV irradiation is observed for the Cu NCs synthesized using the above ligands. This can be explained by the fact that cysteine and cysteamine are soluble in ethanol; thus, dense aggregates of Cu NCs and subsequent AIE effects are not observed. Based on the above observations, we conclude that the formation of Cu NCs is controlled by the fast reduction of Cu ions by GSH and the supersaturation-induced aggregation based on the solubility change of GSH upon solvent mixing.

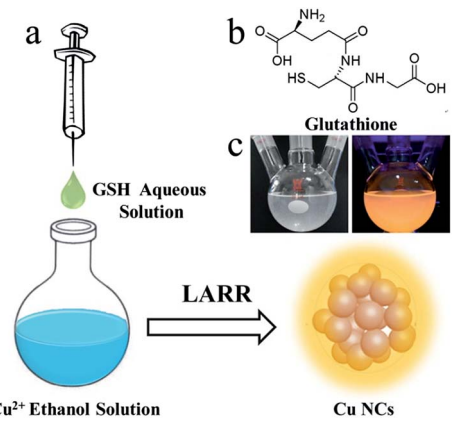

Fig. 1 (a) Schematic illustration of the synthesis of Cu NCs using the LARR method. (b) Structure of GSH. (c) Optical images of a solution of Cu NCs under daylight and UV light.

Characterization of Cu NCs

Fig. 2a shows typical transmission electron microscopy (TEM) images of the Cu NCs. Quasi-spherical nanoparticles with diameters in the range of 50 to 80 nm can be recognized (Fig. 2a), suggesting that the as-synthesized samples are monodisperse. Within a certain nanoparticle, small-sized Cu NCs with an average diameter of 2.3 nm are embedded rather than crystalline Cu. The structure is formed during the ligand-assisted reduction and reprecipitation process, in which the fast reduction of Cu^{2+} by GSH and the supersaturation-induced aggregation triggered by the change in GSH solubility upon solvent mixing occur. The Cu NCs are synthesized and self-assemble within a single nanoparticle, which is driven by the difference in Cu NC solubility in good (water) and poor (ethanol) solvent. The XRD spectrum (Fig. S1†), which shows only a broad peak at around 20°, confirms the poor crystallizability of the Cu NCs. The composition of the Cu NCs was studied by XPS, and all the expected constituent elements of the

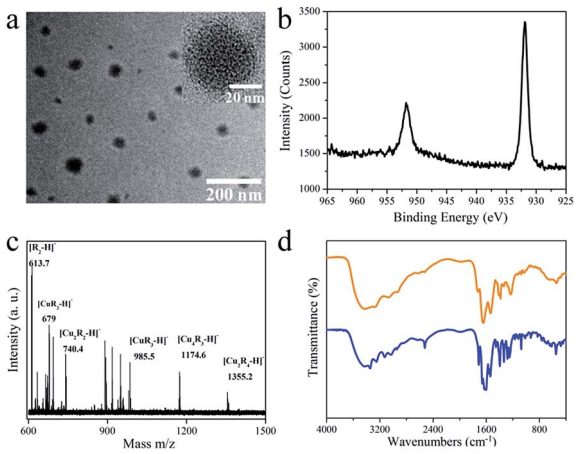

Fig. 2 Characterization of Cu NCs. (a) TEM image (inset shows the HRTEM image). (b) XPS spectrum of Cu 2p electrons. (c) MALDI-TOF MS spectrum of Cu NCs. (d) FTIR spectra of Cu NCs (orange line) and GSH (blue line).

composite (C, O, N, S and Cu) were detected (Fig. S2†). To study the valence state of Cu, the Cu 2p XPS spectrum was recorded (Fig. 2b). The reduction of Cu ions by GSH is demonstrated by the absence of typical Cu^{2+} peaks around 942 eV. The two intense peaks around 932 and 952 eV belong to the $2p_{1/2}$ and $2p_{2/3}$ electrons of metallic copper.[27–29] The valence of Cu lies between 0 and +1, with Cu atom in the core and Cu^{+} located at the surface or bound to the ligands. To determine the ratio of Cu to GSH in the as-synthesized Cu NCs, XPS and TGA were conducted. The molecular ratio of Cu to S was determined to be 3 : 1 based on the XPS results. As shown in the TGA curve of the Cu NCs (Fig. S3†), the Cu NCs are thermally stable in the temperature range of 30 °C to 185 °C, with more than 96% of the weight preserved. A sharp decrease in weight is observed in the temperature range of 200 °C to 400 °C. This weight loss is attributed to the decomposition of GSH ligands. Only 41% of the weight is retained after heating to 800 °C. The ratio of Cu to GSH was calculated to be ~3.2, which is consistent with the XPS measurements. MALDI-TOF MS analysis was carried out to determine the composition of the Cu NCs (Fig. 2c). The two major peaks located at m/z = 1355.2 and 1174.7 in Fig. 2c correspond to $[Cu_2R_4{}^{-}H]^{-}$ and $[Cu_3R_3{}^{-}H]^{-}$, respectively, where R = $C_{10}H_{16}O_6N_3S$. FTIR was further used to study the interaction between GSH and the Cu NCs (Fig. 2d). No other new or obliterated peaks are observed in the FTIR spectra of GSH and Cu NCs, except for the disappearance of the peak at 2524 cm^{-1}, which corresponds to the S–H stretching vibration mode of GSH.[30] This indicates that GSH is connected to the Cu NCs *via* Cu–S bonds without connections with other chemical groups, such as $-NH_2$ and –COOH. The above results strongly support our hypothesis that nanoparticles containing small-sized Cu NCs are synthesized *via* the GSH-assisted reduction of Cu^{2+} and reprecipitation controlled by the injection of GSH dissolved in good solvent into poor solvent.

PL properties of the Cu NCs

Fig. 3a shows the UV-visible absorption spectrum of the as-synthesized Cu NCs. The spectrum is rather structure-less with a vague peak around 365 nm. This peak can be ascribed to the inter-band electronic transitions of the Cu NCs. The absence of surface plasmon resonance peaks around 560–600 nm excludes the formation of large copper particles.[30] As shown in Fig. 3a, an intense orange emission peak at 615 nm and a PL excitation (PLE) peak around 350 nm were recorded, resulting in a PL QY as high as 29.7%. This QY is higher than those of most reported Cu NCs and better than that of Cu NCs synthesized through reprecipitation by directly injecting Cu NCs into poor solvents.[12] The as-synthesized Cu NCs can be feasibly processed into solid sates by evaporating the solvent, producing luminescent NC powders (inset of Fig. 3a). It is worth noting that a blue shift from 615 to 600 nm is observed in the peak in the PL spectra of the Cu NCs in solution and powder states. After processing into the power state, the average inter-atomic distance can be increased by increasing the ratio of inter-NC metallophilic interactions to intrinsic intra-NC metallophilic interactions. This leads to the promotion of emission

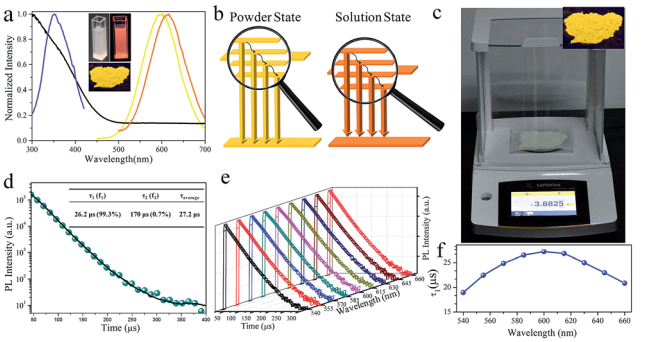

Fig. 3 (a) UV-visible absorption (black line), PL (orange line) and PLE (purple line) spectra of the as-synthesized Cu NCs, PL spectrum of Cu NC powder (yellow line), and photos under irradiation by daylight and UV light. (b) Schematic Illustration of the energy level of Cu NCs with powder and solution state; (c) photos of sample (more than 3 g) obtained from large-scale synthesis and its photo showing orange emission under UV radiation (insert); (d) PL decay profiles of Cu NC powder, showing a nearly monoexponential decay, with PL lifetimes (τ_{1-2}, μs) and fractions (f_{1-2},%) obtained from the fitting of bio-experimental data shown in the inset; (e) PL decay profiles and (f) PL lifetimes of Cu NC powder detected at different emission wavelength.

energy and a blue shift in the emission peak of the Cu NCs, as depicted in Fig. 3b. The LARR synthesis can easily produce grams of orange-emissive solid materials with PL QY as high as 48% through batch experiments simply by scaling up the synthesis (Fig. 3c). As stated in the introduction, the AIE can be ascribed to the enhanced NC metallophilic interactions and the restriction of ligand vibration and rotation. Similar to most of the reported AIE studies, using overdosed poor solvents to trigger the AIE of metal NCs, the aggregation of Cu NCs caused by the supersaturation of ligands hinders the flexibility of GSH on the surface of the clusters, which results in the suppression of non-radiative decay channels and promoted PL QY. Moreover, metal defects in the Cu NCs are deliberately created during the LARR process. Before reaction, Cu^{2+} is dissolved into ethanol and allowed to coordinate with Cu, which alters the coordination environment of Cu atoms and the surface properties of Cu clusters.[25] This may create more metal detects and prevent their passivation during synthesis, which allows more exited electrons to be transferred to a metal defect-related intermediate state, leading to a PL QY higher than that of aggregated metal NCs prepared by simply dispersing clusters in excess poor solvent. Our results are in agreement with Wu and co-authors, who found that the PL QY can be tuned by adjusting the number of metal defects on Cu NCs.[25]

Nearly monoexponential PL decay behavior of Cu NCs

To gain more insight into the dynamics of exciton recombination, the PL decay curves of the Cu NCs were measured (Fig. 3d). The decay curves can be fit biexponentially with a shorter PL lifetime (τ_1) of 26.2 μs (99.3%) and a longer PL lifetime (τ_2) of 170 μs (0.7%). The biexponential decay behavior indicates that two species are involved in the emission of the Cu NCs. In light of the study of the mechanisms of metal NCs with AIE

phenomena, metal defect-related emissions are the main contributors to the improved PL QY. Compared to reported metal NCs, the decay of the Cu NCs shows a nearly monoexponential behavior, with τ_1 accounting for more than 99% of the decay, which can be related to exciton recombination from metal defect-related emission. Monoexponential decay often indicates that radiative processes are dominant, and a PL QY of unity is expected to be achieved.[31] The PL QY of the Cu NCs is only 48%; thus, around 50% of the clusters are assumed to be located in dark states because they failed to relax into the metal defect-related states. The PL decay of Cu NCs at different emission wavelengths were recorded and are shown in Fig. 3e. Nearly monoexponential behavior is observed at different detection wavelengths, with τ_1 accounting for more than 99% of decay, as shown in Table S1.† This indicates that all emissions are from the same metal defect-related state. The PL lifetimes of τ_1 detected at different wavelengths are presented in Fig. 3f, indicating wavelength-dependent properties. This indicates the trapping of multiple electrons during the recombination process of the Cu NCs, as indicated schematically in Fig. 3b. A maximum value of τ_1 is obtained at the wavelength of 600 nm, the same as the position of the peak in the PL spectrum. This suggests that emission from the peak corresponds to the lowest energy level of the metal defect-related states.[26]

Applications for LEDs

The luminescent powder with high PL QY and potential for large-scale synthesis provides an opportunity to explore its application in LEDs. The toxicity of Cu NCs is an important consideration for practical applications. In this study, Cu NC cytotoxicity was evaluated by MTS assay in 3T3 fibroblasts. As shown in Fig. S4,† only a slight decrease in cell viability is observed after incubation for 24 h, and over 95% cell viability is retained by cells incubated with Cu NCs at concentrations as high as 12 μg mL^{-1}. This suggests that the as-synthesized Cu NCs have low toxicity. To demonstrate potential illumination applications, white LEDs were fabricated by combing blue-emissive commercial phosphors (BMA) and orange-emissive Cu NCs with UV-LED chips. Fig. 4a shows photographs of the blue- and orange-emitting powders taken under UV illumination together with their PL and PLE spectra. The emission of the blue and orange powders covers the full visible spectral range from 400 to 700 nm, demonstrating the potential to generate white light. Moreover, a wide overlap (from 300 to 400 nm) is observed in the PLE spectrum; thus, both phosphors can be excited using a single UV light. Blue, orange and white LEDs were fabricated by integrating BMA, Cu NCs and a mixture of both with UV-LED chips (emitting light centered at 370 nm, as shown in Fig. S5†). Fig. 4b and c–f show photographs of the devices and the emission spectra of blue, orange and white LEDs, respectively. Moreover, the Commission Internationale de L'Eclairage (CIE) chromaticity positions of the LEDs can be tuned form blue (0.19, 0.14) to white light (0.33, 0.32) towards orange (0.45, 0.48) by systematically controlling the weight ratio of blue- to orange-emitting phosphors. After optimization, white LEDs with CIE chromaticity coordinates of (0.33, 0.32), close to sunlight,[32] a high CRI of 89, and a color temperature of 4519 K were fabricated.

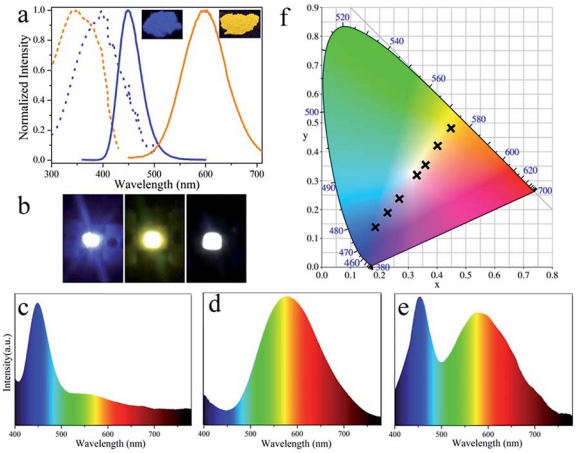

Fig. 4 (a) Optical spectra of phosphors with photographs under UV illumination shown as insets: PL (solid line, excited at 365 nm) and PLE (dotted line, detected at the corresponding PL peaks) of BMA (blue) and Cu NCs (orange). (b) Photographs of operating blue, orange and white LEDs. (c–e) Emission spectra of blue, orange and white LEDs, respectively. (f) CIE chromaticity coordinate diagram of LEDs fabricated by mixing different ratios of blue and orange phosphors.

Conclusions

In summary, a straightforward LARR method for synthesizing brightly luminescent Cu NCs is proposed. This method is low in cost, avoids the use of toxic metals or rare earth elements, and can be conveniently scaled up for large-scale synthesis. The as-synthesized Cu NCs show a PL QY as high as 48%, which is attributed to the AIE effect caused by supersaturation-induced aggregation and the protection of metal defects by coordination between ethanol and Cu. Moreover, the PL decay curves show nearly monoexponential behavior due to the existence of metal defect-related states. The homogeneity of PL decay behavior at different detection wavelengths and the wavelength-dependent PL lifetimes demonstrate that the emissions of the Cu NCs come from the same metal defect-related state, and multiple electrons are trapped during the recombination process. After integrating the orange-emissive Cu NCs and blue-emissive phosphors with UV-LED chips, we developed a series of LEDs with tunable emission color from blue to white to orange. A white light with favorable CIE coordinates (0.33, 0.32), CRI (89) and color temperature (4519 K) is achieved. The availability of luminescent Cu NCs adds a new family member to SLMs and will open the door to numerous applications in sensing, bioimaging, security printing and LEDs.

Experimental

Materials

Chemicals including copper(II) nitrate [$Cu(NO_3)_2$] and GSH were purchased from Sigma-Aldrich, USA. L-Cysteine hydrochloride anhydrous and cysteamine were purchased from Kermel,

Tianjin, China. Commercial blue phosphors ($BaMgAl_{10}O_7$:Eu, BMA) were obtained from Shenzhen Looking Long technology Co. Ltd. Silicone resin components OE-6551A and OE-6551B were purchased from Dow Corning Co.

Synthesis of Cu NCs

Cu NCs were synthesized through a LARR process. Typically, 0.5 mL of GSH aqueous solution (250 mM) was injected into 9.5 mL ethanol solution containing 5 mM dissolved Cu^{2+} under vigorous stirring. The color of the mixture changed from intense blue to black to dark green and finally to milky as the stirring time increased. Finally, the products were centrifuged at 500 krpm to remove the large yellow particles, and the supernatant solution was collected. Cu NC powder was prepared by discarding the solvent and drying in an oven.

Fabrication of LEDs

To fabricate blue or orange LEDs, 0.1 g of blue phosphor or Cu NC powder was mixed with 0.1 g of silicone resin OE-6551A. To fabricate WLEDs, 0.1 g of blue phosphor and 0.4 g Cu NC powder were mixed with 0.1 g of OE-6551A. The above mixtures were then dried at 50 °C for 1 h and mixed with 0.2 g OE-6551B powder. After coating onto GaN LED chips, the emission wavelength peaked at 370 nm.

Characterization

UV-visible and PL spectra were collected using a Varian Cary 50 UV-visible spectrophotometer and a Varian Cary Eclipse fluorescence spectrometer, respectively. TEM images were recorded on a Philips CM 20 microscope. XPS measurements of Cu NCs were conducted on an ESCALAB-MKII 250 photoelectron spectrometer (Thermo, USA). MALDI-TOF MS spectra were recorded using a mass spectrometer (Bruker Daltonics, USA). FTIR spectra of GSH and Cu NCs were recorded on a Perkin-Elmer Spectrum 100 FTIR spectrometer. Time-resolved PL decay curves were collected on a time-correlated single-photon counting setup under excitation with a 320 nm laser. PL decay curves were fitted with two-exponential functions in the form of eqn (1):

$$I(t) = B_1 e^{-\frac{t}{\tau_1}} + B_2 e^{-\frac{t}{\tau_2}},\ B_1 + B_2 = 1, \quad (1)$$

where τ_1 and τ_2 represent the decay constants, and B_1 and B_2 represent the normalized amplitudes of each component. The amplitude-weighted average lifetime of the entire photoluminescence decay process was calculated using eqn (2):

$$\tau = \frac{B_1\tau_1^2 + B_2\tau_2^2}{B_1\tau_1 + B_2\tau_2}. \quad (2)$$

Absolute PL QY was determined using a spectrofluorometer (FLS920P, Edinburgh Instruments) equipped with an integrating sphere. The LED parameters, including CIE color coordinates, CRI, and color temperature, were recorded using a high-accuracy array rapid spectroradiometer (Haas-2000, Everfine Co., Ltd., China) equipped with an integrating sphere.

Conflicts of interest

There are no conflicts to declare.

Acknowledgements

This work is supported by the National Natural Science Foundation of China (21804030).

References

1 C.-L. Liu, R.-L. Zhang, C.-S. Lin, L.-P. Zhou, L.-X. Cai, J.-T. Kong, S.-Q. Yang, K.-L. Han and Q.-F. Sun, *J. Am. Chem. Soc.*, 2017, **139**, 12474–12479.
2 W. Guan, W. Zhou, J. Lu and C. Lu, *Chem. Soc. Rev.*, 2015, **44**, 6981–7009.
3 A. Fernández and M. Vendrell, *Chem. Soc. Rev.*, 2016, **45**, 1182–1196.
4 G. G. Dias, A. King, F. de Moliner, M. Vendrell and E. N. da Silva Júnior, *Chem. Soc. Rev.*, 2018, **47**, 12–27.
5 H. Sun, S. Liu, W. Lin, K. Y. Zhang, W. Lv, X. Huang, F. Huo, H. Yang, G. Jenkins, Q. Zhao and W. Huang, *Nat. Commun.*, 2014, **5**, 3601.
6 K. Jiang, Y. Wang, C. Cai and H. Lin, *Adv. Mater.*, 2018, **30**, 1800783.
7 J. Lee, H.-F. Chen, T. Batagoda, C. Coburn, P. I. Djurovich, M. E. Thompson and S. R. Forrest, *Nat. Mater.*, 2015, **15**, 92.
8 Z. Wang, F. Yuan, X. Li, Y. Li, H. Zhong, L. Fan and S. Yang, *Adv. Mater.*, 2017, **29**, 1702910.
9 H. V. Demir, S. Nizamoglu, T. Erdem, E. Mutlugun, N. Gaponik and A. Eychmüller, *Nano Today*, 2011, **6**, 632–647.
10 H. Terraschke and C. Wickleder, *Chem. Rev.*, 2015, **115**, 11352–11378.
11 L. Wang, R.-J. Xie, T. Suehiro, T. Takeda and N. Hirosaki, *Chem. Rev.*, 2018, **118**, 1951–2009.
12 Z. Wang, B. Chen, A. S. Susha, W. Wang, C. J. Reckmeier, R. Chen, H. Zhong and A. L. Rogach, *Adv. Sci.*, 2016, **3**, 1600182.
13 Z. Wang, Q. Jingjing, X. Wang, Z. Zhang, Y. Chen, X. Huang and W. Huang, *Chem. Soc. Rev.*, 2018, **47**, 6128–6174.
14 L. Jing, S. V. Kershaw, Y. Li, X. Huang, Y. Li, A. L. Rogach and M. Gao, *Chem. Rev.*, 2016, **116**, 10623–10730.
15 Q. Yao, T. Chen, X. Yuan and J. Xie, *Acc. Chem. Res.*, 2018, **51**, 1338–1348.
16 Q. Yao, V. Fung, C. Sun, S. Huang, T. Chen, D.-e. Jiang, J. Y. Lee and J. Xie, *Nat. Commun.*, 2018, **9**, 1979.
17 X. Kang, M. Zhou, S. Wang, S. Jin, G. Sun, M. Zhu and R. Jin, *Chem. Sci.*, 2017, **8**, 2581–2587.
18 T. Higaki, C. Liu, M. Zhou, T.-Y. Luo, N. L. Rosi and R. Jin, *J. Am. Chem. Soc.*, 2017, **139**, 9994–10001.
19 I. Chakraborty and T. Pradeep, *Chem. Rev.*, 2017, **117**, 8208–8271.
20 J. Mei, N. L. C. Leung, R. T. K. Kwok, J. W. Y. Lam and B. Z. Tang, *Chem. Rev.*, 2015, **115**, 11718–11940.
21 J. Luo, Z. Xie, J. W. Y. Lam, L. Cheng, H. Chen, C. Qiu, H. S. Kwok, X. Zhan, Y. Liu, D. Zhu and B. Z. Tang, *Chem. Commun.*, 2001, 1740–1741.

22 Z. Wang, Y. Xiong, S. V. Kershaw, B. Chen, X. Yang, N. Goswami, W.-F. Lai, J. Xie and A. L. Rogach, *Chem. Mater.*, 2017, **29**, 10206–10211.
23 Z. Luo, X. Yuan, Y. Yu, Q. Zhang, D. T. Leong, J. Y. Lee and J. Xie, *J. Am. Chem. Soc.*, 2012, **134**, 16662–16670.
24 X. Jia, J. Li and E. Wang, *Small*, 2013, **9**, 3873–3879.
25 Z. Wu, H. Liu, T. Li, J. Liu, J. Yin, O. F. Mohammed, O. M. Bakr, Y. Liu, B. Yang and H. Zhang, *J. Am. Chem. Soc.*, 2017, **139**, 4318–4321.
26 Y. Liu, D. Yao and H. Zhang, *ACS Appl. Mater. Interfaces*, 2018, **10**, 12071–12080.
27 Z. Wang, B. Chen and A. L. Rogach, *Nanoscale Horiz.*, 2017, **2**, 135–146.
28 Z. Wang, Y.-e. Shi, X. Yang, Y. Xiong, Y. Li, B. Chen, W.-F. Lai and A. L. Rogach, *Adv. Funct. Mater.*, 2018, **28**, 1802848.
29 Z. Wu, J. Liu, Y. Gao, H. Liu, T. Li, H. Zou, Z. Wang, K. Zhang, Y. Wang, H. Zhang and B. Yang, *J. Am. Chem. Soc.*, 2015, **137**, 12906–12913.
30 X. Liu and D. Astruc, *Coord. Chem. Rev.*, 2018, **359**, 112–126.
31 S. F. Wuister, I. Swart, F. van Driel, S. G. Hickey and C. de Mello Donegá, *Nano Lett.*, 2003, **3**, 503–507.
32 C. C. Lin, A. Meijerink and R.-S. Liu, *J. Phys. Chem. Lett.*, 2016, **7**, 495–503.